Numerical simulation and validation of a high head model Francis turbine at part load operating condition

Rahul Goyal
Ph. D. Student, Department of Mechanical and Industrial Engineering, Indian Institute of Technology Roorkee, India;
Email: goel.rahul87@gmail.com
Chirag Trivedi
Postdoctoral Fellow, Department of Mechanical and Industrial Engineering, Indian Institute of Technology Roorkee, India;
Email: chirag.trivedi@ltu.se
B. K. Gandhi
Professor, Department of Mechanical and Industrial Engineering, Indian Institute of Technology Roorkee, India. Email: bkgmefme@iitr.ernet.in (author for correspondence)
Michel J. Cervantes
Professor, Division of Fluid and Experimental Mechanics, Department of Engineering Sciences and Mathematics, Luleå University of Technology, Sweden
and
Professor, Water Power Laboratory, Department of Energy and Process Engineering, Norwegian University of Science and Technology, Norway.
Email: Michel.Cervantes@ltu.se

Abstract

Hydraulic turbines are operated over an extended operating range to meet the real time electricity demand. Turbines operated at part load have flow parameters not matching the designed ones. This results in unstable flow conditions in the runner and draft tube developing low frequency and high amplitude pressure pulsations. The unsteady pressure pulsations affect the dynamic stability of the turbine and cause additional fatigue. The work presented in this paper discusses the flow field investigation of a high head model Francis turbine at part load: 50% of the rated load. Numerical simulation of the complete turbine has been performed. Unsteady pressure pulsations in the vaneless space, runner, and draft tube are investigated and validated with available experimental data. Detailed analysis of the rotor stator interaction and draft tube flow field are performed and discussed. The analysis shows the presence of a rotating vortex rope in the draft tube at the frequency of 0.3 times of the runner rotational frequency. The frequency of the vortex rope precession, which causes severe fluctuations and vibrations in the draft tube, is predicted within 3.9% of the experimental measured value. The vortex rope results pressure pulsations propagating in the system whose frequency is also perceive in the runner and upstream the runner.

Keywords: Numerical simulation, Francis turbine, part load, pressure pulsation, rotor-stator interaction, vortex rope.

Nomenclature

BEP= best efficiency point

D=diameter of runner [m]

GVO= guide vane's opening [°]

FFT= fast Fourier transform

f=observed frequency [Hz]

f_n= runner rotational frequency [Hz]

f*= Normalised frequency [-]

f_{rh}= Rheingans (vortex rope) frequency [Hz]$\equiv f/3.6$

g= 9.821465 [m s^{-2}], as tested and measured at NTNU

H=head [m]

N= Sampling length

n=runner speed [rev s^{-1}]

n_{ED}= speed factor [-], $$n_{ED} = \frac{nD}{\sqrt{gH_M}}$$

n_s = specific speed [-], $$n_s = \frac{\left(n_P \cdot \dfrac{\pi}{180}\right)\sqrt{Q_P}}{\left(2 \cdot g \cdot H_P\right)^{\frac{3}{4}}}$$

Δp= pressure difference across the turbine [Pa]

$\tilde{p}$ = acquired pressure signal [kPa]

$\bar{p}$ =mean pressure [kPa]

p^* = fluctuating pressure [kPa]

p=pressure [kPa]; harmonic order (1, 2,..)

P=power [MW]

Q=flow rate [m^3 s^{-1}]

q_{ED}= discharge factor [-], $$q_{ED} = \frac{Q}{D^2\sqrt{gH_M}}$$

R=runner inlet radius[m]

GVO= Guide vane's opening [degree]

RSI= rotor stator interactions

RVR= rotating vortex rope

TS = time step

TKE=Turbulence kinetic energy

t= time [s]

UPW = upwind

X= discrete quantity

$\overline{\overline{X}}$ =average value

λ= wavelength [m]

α= angular vane/blade position [º]

ω=angular velocity [rad s^{-1}]

η$_h$=Hydraulic efficiency [%]

Introduction

Electricity produced by different types of hydraulic turbines is injected to the grid network to meet the real time demand. Variable electricity demand and generation may disrupt the grid network. Hydropower is used to meet the real time electricity demand and maintain the grid stability. Thus, the hydraulic turbines are required to operate away from the best efficiency point (BEP) [1-2]. At part load operation, Francis turbine experiences both low and high frequency pressure fluctuations [3]. The high frequency pressure pulsations are developed by the rotor-stator interaction (RSI), and the low frequency pressure pulsations are developed by the vortex breakdown in the draft tube [4-6]. Experimental and numerical investigations on Francis turbines showed that the amplitude of the pressure fluctuations is moderate at the BEP whereas at the part load, the amplitude becomes significant [7-8].

The pressure pulsation frequency depends on the number of blades, number of guide vanes, and the runner angular speed. A high amplitude pressure pulse is developed as a blade passes a guide vane. The amplitude of the pulsation depends on the guide vanes opening. The RSI is a periodical phenomenon for constant runner angular speed [3]. In reality, some variation occurs due to the frequency variation on the grid. The pressure amplitude may depend on the wake generated from the trailing edge of the interacting guide vane. A non-uniform variation of the pressure due to RSI may cause variation of the shaft torque [3, 9-12].

In a Francis turbine, the runner is designed for an attached flow at the BEP discharge. At part load, the low flow entering the rotating blade passages from the guide vanes generates vortices and separation in the passages due to mismatch between the flow angle and the blade inlet angle. Blade trailing edge also develops vortices. The mismatch flow angle and the vortices cause vortex breakdown downstream the runner [13-15]. The frequency of the vortex breakdown is generally 0.2 to 0.4 times of the runner rotational frequency. Pressure waves at this frequency may be observed at other locations in the turbine such as runner, vaneless space, and spiral casing [16-17]. In an analysis of the swirling flow downstream of a Francis turbine runner, the flow stability characteristics was observed to change due to a decrease in discharge. The swirling flow downstream a runner in the draft tube cone reaches a critical state away

from the BEP. For larger discharge, the swirling flow is supercritical, and thus it is not able to sustain axis-symmetrical perturbations and develops a plunging mode in the draft tube. However, at partial discharge, the flow becomes subcritical and sustains axis-symmetric perturbations [18].

A summary of the numerical studies conducted to investigate the Francis turbines is presented in Table 1. Most of the simulations were performed using unsteady Reynolds-averaged Navier-Stokes (RANS) models and with relatively coarse mesh [19-21]. The numerical results are generally compared with experimental measurements which show that the difference between the two depends on the numerical parameters such as turbulence models, discretization scheme etc. Further, the time dependent parameters and frequency may also cause a larger difference in experimental and numerical results for transient simulation [12, 20-22].

Table 1. Summary of numerical simulations of hydraulic turbines

Author	Domain	Elements/ Node (x10^6)	y$^+$ [-]	Code	Analysis type	Advection scheme	Convergence control	Turbulence model
Zoberi et al. 2006 [12]	Complete turbine	0.910	average 60-270	CFX	Transient TS-0.5°	1storder	Residual ≥10E-3	Std k-ε
Buntic et al. 2005 [19]	Draft tube	1.000	≈50	Own	Transient TS-0.01s	2ndorder	--	Ext k-ε Chen and Kim, VLES
H. Wallimann et al. 2015 [20]	Complete turbine	13.1	-	CFX	Transient	High res	--	SST model
Wu et al. 2007 [21]	Complete turbine	2.500	≥40	CFX	Transient	High res	--	Std & Mod k-ω, SST, Std k-ε
Ciocan et al. 2007 [22]	Runner & Draft tube	0.920	--	CFX	Transient TS-1°	High res	RMS residual ≥10E-4	Std k-ε
Staubli et al.1999 [23]	Draft tube	0.493	11-330	CFX-TASC	Transient TS-0.3s	1storder	RMS residual ≥10E-4	Std k-ε
Luis et al. 2003 [24]	Distributor	2.621	≤2	CFX	Steady State	1storder	RMS residual ≥10E-5	Std k-ε, k-ω, KE 1-equation

Widmer et al. 2011 [25]	Complete turbine	5.000	--	CFX	Transient TS-1 to 5°	High res	RMS residual ≥5E-5	Std k-ε
Peter Mossinger et al. 2015 [26]	Complete turbine	20	≈53	CFX	Transient	High res	Residual ≥10E-3	k-ω SST, k-ε, Reynold stress model
D Jošt et al. 2015 [27]	Complete turbine	13.1	≥49.3	CFX	Transient	High res	--	Std k-ε, SST
This paper	Complete turbine	12.029	Casing ≤65 Runner ≤11 Draft tube≤40	CFX	Transient TS-0.5°	High res, 2nd order UPW	RMS residual ≥10E-5	Std k-ε and SST k-ω

The vortex breakdown is a complex flow phenomenon. Experiments are generally conducted to visualise the vortex rope or study the unsteady pressure pulsations in the draft tube. The available commercial code for computational fluid dynamics (CFD) together with the low computer cost made it an important tool for obtaining additional information concerning the structure of the breakdown, as well as identifying various parameters affecting its occurrence and development. The simulation of a turbulent swirling flow, however, is a challenging task, and an accurate numerical calculation of the flow parameters requires a careful choice of turbulence closure method. Many investigators have performed turbulent swirling flow predictions using RANS equation with various turbulence models [19-21]. The flow physics were well captured by the RANS equations at part load operating conditions and vortex breakdown was found as the source of instability of the flow at these operating points [16-18].

In Francis turbines, the vortex rope is generally present at a discharge of 0.5 to 0.85 times the discharge at BEP [16]. At these operating conditions, a hydraulic turbine experiences unstable flow conditions. Both high and low frequency pressure pulsations affect the dynamic stability of the turbine. Very few experimental and numerical investigations [16, 20, 24, and 26] were performed at part load operating conditions, particularly in the range 50 - 70% of the BEP load, where the amplitude of the low frequency pressure pulsations in the draft tube was reported high. The maximum difference between the experimental and numerical simulation results is usually seen at these conditions [22].

Experimental measurements for a large range of operating conditions of a high head model Francis turbine were performed by Trivedi et al. 2013 [3] ; the constant efficiency hill diagram is shown in Fig.1. They observed the maximum hydraulic efficiency of 93.4% at a speed factor (n_{ED}) of 0.18 and a discharge factor (q_{ED}) of 0.15 for guide vane's opening (GVO) of 9.84º, which is marked as BEP. The numerical validation of experimental data at high load (GVO=12.44°), BEP (GVO=9.84°), and low load (GVO=3.91°) was also discussed and published by Trivedi et al. 2013 [3]. Trivedi et al. 2013 [3] have measured the pressures inside the turbine using six pressure sensors as shown in Fig. 2. One of the sensors was mounted in the vaneless space (VL01) to measure the pressure at the runner inlet, two sensors were mounted on the pressure side of the blade (P41 and P71) and one sensor was mounted on the suction side of the blade (S51). The remaining two sensors, DT11 and DT21, were mounted in the draft tube cone at the same distance from the runner outlet and both sensors were located 180º from each other. They also measured the pressure at the inlet pipeline by mounting two pressure transmitters, PTX1 and PTX2, at 4.87 and 0.87 m upstream of the turbine inlet, respectively. No significant amplitude of low frequency (vortex rope) was reported at the low load. Trivedi et al. 2013 [13] have also performed the simulations for three operating points, namely high load, BEP and very low load using two turbulence model standard k-ε and SST k-ω model and compared the numerical prediction with experimental measurements. In all cases, the deviation of numerical hydraulic efficiencies as compared to experimental values was lower for standard k-ε model as compared to SST k-ω model. However, investigator [26] reported that low frequency pulsations may be better predicted by SST k-ω model.

. As mentioned before, the low load operating condition used in previous study by Trivedi et al. 2013 [3] was not feasible to perform for vortex rope in the draft tube. Therefore, a new operating condition was chosen for the part load (GVO= 6.72°). The present work aims to numerically simulate the model turbine tested by Trivedi et al. 2013 [3] at 50% load and compare the numerical results with the experimental data presented by the authors in an another communication [28]. The lack of numerical validation at this operating point motivates to carry out the simulation with two difference turbulence models (standard k-ε and SST k-ω) for the present case. The results from both models are compared with experimental data for some specific points in the flow domain. The best numerical model is further used for the analysis of the dominant frequencies present in the stationary (vaneless space and draft tube) and rotating (runner blades) domain. Moreover, the detailed analysis of the pressure-time data is aimed to investigate the effect of the RSI and vortex breakdown phenomena in the stationary and rotary domains. Detailed analysis of the pressure-time data determined for the vaneless space, blade pressure and suction side, and draft tube cone are presented. Flow field has been analysed in detail to investigate RSI, blade loading, and vortex breakdown in the draft tube.
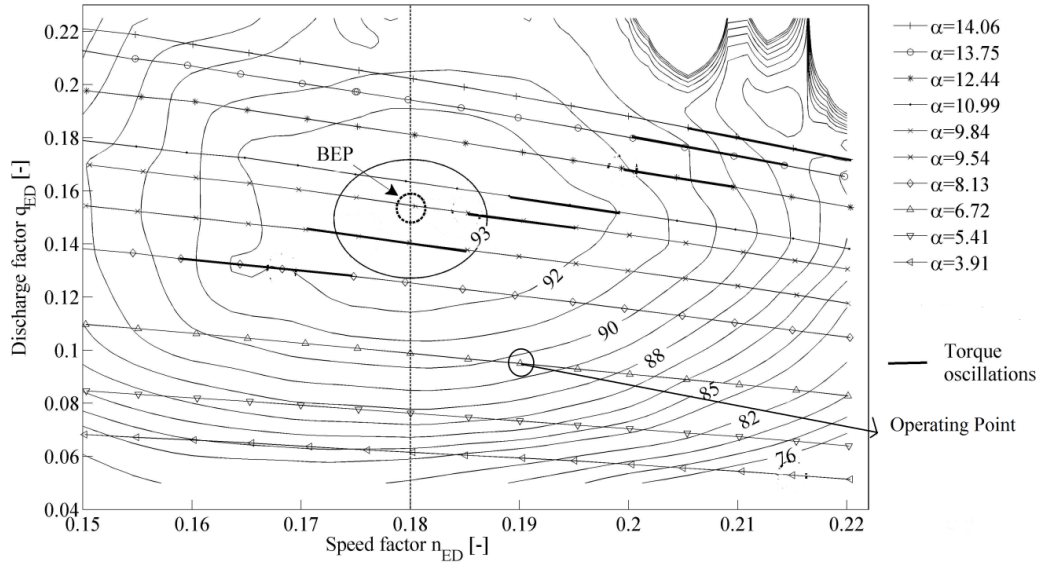
Fig. 1: Constant efficiency hill diagram of the high head model Francis turbine (D_M= 0.349 m, H_M=12 m, N_{QE} = 0.27) [3];
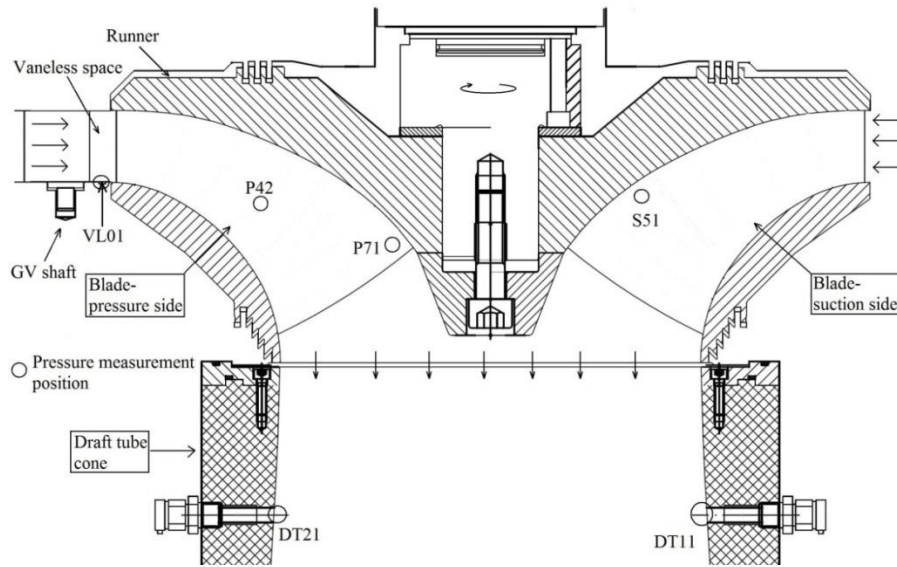

Fig. 2 Locations of the pressure sensors and numerical points to record pressure-time data; positions VL01, P42, P71, S51, DT11, and DT21 were used to compare the numerical results with the experimental data [3].

Numerical model

The computational domain comprises three sub-domains: distributor (stationary domain – I), runner (rotating domain), and draft tube (stationary domain – II). The distributor and draft tube are located upstream and downstream the runner, respectively. Numerical model of the Francis turbine is shown in Fig. 3. Both stationary domains are connected with the runner using a general grid interface (GGI) type interface. The distributor includes spiral casing, 14 stay vanes, and 28 guide vanes. The runner includes hub, shroud, 15 full length blades, and 15 splitters. The draft tube is an elbow type diffuser connected at the runner outlet. The inlet boundary condition was prescribed at the casing inlet and the outlet boundary condition was the pressure at the draft tube outlet.
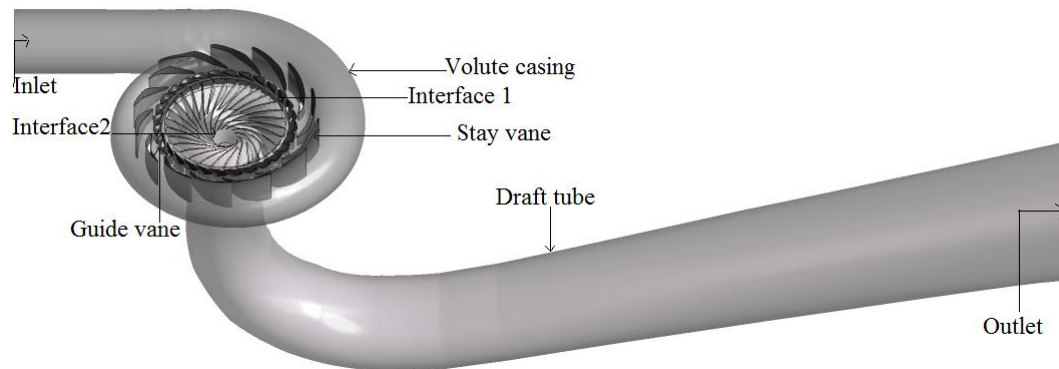

Fig. 3 Computational domain of the model Francis turbine with two interfaces, distributer to runner (interface – 1) and runner to draft tube (interface – 2), 14 stay vanes, 28 guide vanes, runner with 15 full length blades and 15 splitters, and draft tube connected to runner outlet.

Space discretization

A commercial software ANSYS CFX was used to create the numerical model, generate a hexahedral mesh, simulate the flow domain and analyze the results. The mesh was created using three-dimensional structured multi-block technique with ICEM. The mesh was created independently in each subdomain. Figure 4 shows the hexahedral mesh developed in the turbine. A continuous mesh from the spiral casing inlet to the runner inlet was constructed in the distributor. Node spacing, node distribution and element size were uniform at both the interior faces, namely distributor outlet and runner inlet. The same mesh parameters were used to create a continuous mesh in the runner starting from interface–1 to interface-2, i.e., inlet to the outlet of the runner. Hexahedral blocks of the same dimensions were constructed for each blade passage and all the blocks were merged together. The number of nodes, spacing, and element size from hub to shroud were uniform in all the channels; therefore, the grid and quality along the runner circumference or blade-to-blade did not vary. The interface – 2 is placed at the runner outlet and the draft tube inlet. In the draft tube domain, a continuous and coherent mesh was constructed from the inlet to the outlet.
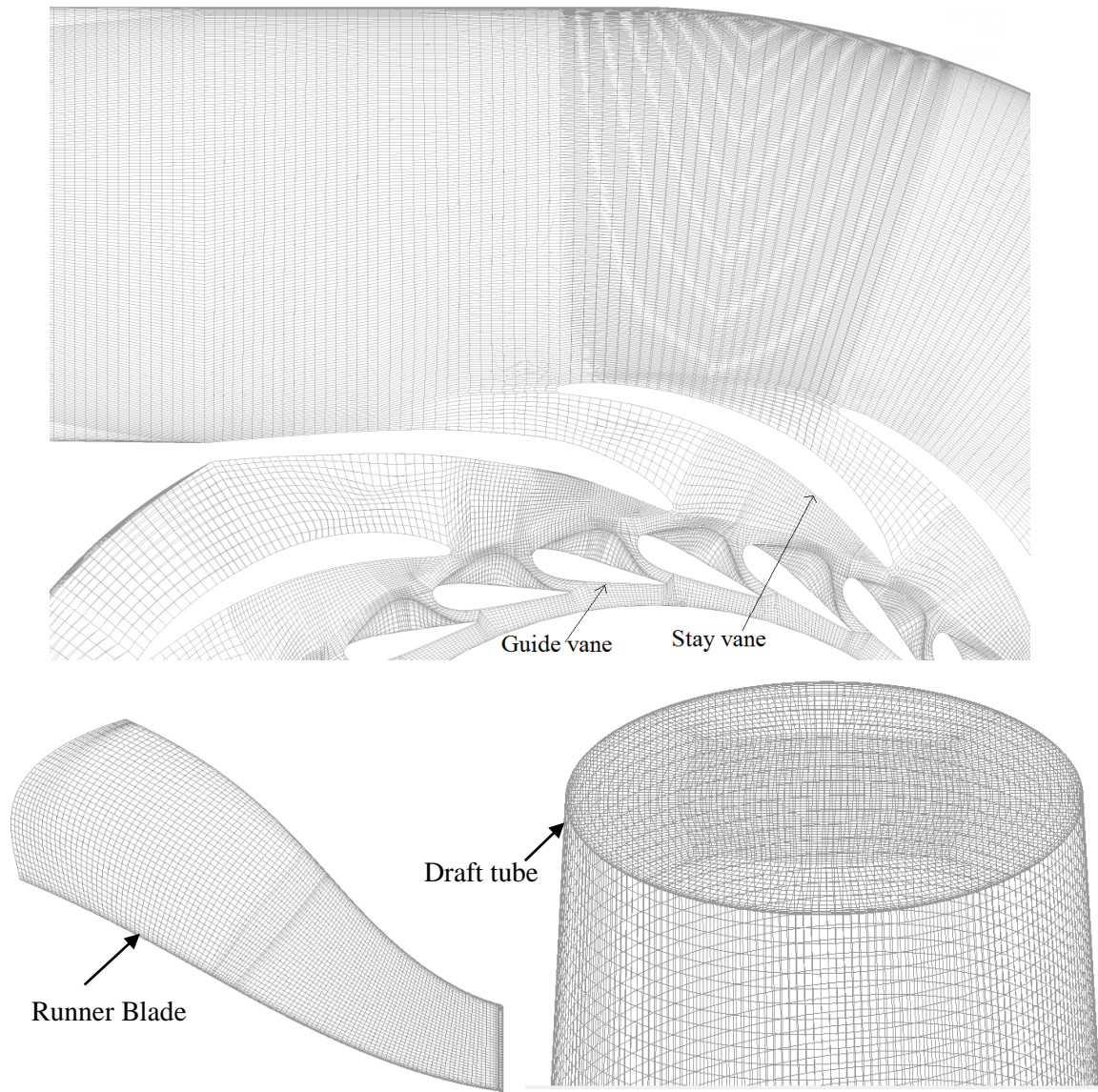
Fig. 4 Hexahedral mesh of the high model Francis turbine

Meshes with three different densities 20.73, 10.94, and 4.83 million nodes, were created to perform mesh independency test by Trivedi et al. 2013 [3]. Table 2 shows the mesh parameters and the quality used for the simulations. Trivedi et al. 2013 [3] reported Grid type G2 as the optimum mesh at BEP. For the present work, Grid type G2 is selected and the quality of the mesh was maintained for the present guide vane opening (GVO) of 6.72°. The other parameter, total nodes, node spacing, quality of the elements, and edge parameters etc., were identical to these reported by Trivedi et al. 2013 [3].

Table 2 Grid densities used in mesh independency test [3]

Grid type	G$_1$	G$_2$	G$_3$
Distributor	8528119	3255676	2073735
Runner	7527320	4047898	1766246
Draft tube	4679404	3639241	991512
Total nodes (million)	20.73	10.94	4.83
Quality of the elements	0.25-1.0	0.25-1.0	0.25-1.0
Element angle (minimum)	38	41	23
Element aspect ratio	≥0.40	≥0.35	≥0.10
Node incremental ratio	0.07;1.5x	0.25;1.3x	1.65;2.0x
Y$^+$	≤40	≤65	≤285

Boundary conditions and solution set-up

The available literature [2, 10-19] shows that the mass flow inlet and pressure outlet are the most appropriate boundary conditions to simulate Francis turbines. The same type of boundary conditions were selected for the current simulations. The outlet of the draft tube on the test rig is inclined by 15.2° from the horizontal plane upwards and connected to the downstream tank. The numerical boundary was selected as an opening-type with a prescribed steady water pressure corresponding to the available water level in the downstream tank. Using this boundary type, momentum can cross the boundary and re-enter the draft tube). Unsteady simulations were performed. The runner rotational frequency for the present case is 5.94 Hz. To investigate the vortex breakdown, which frequency is generally 0.2 to 0.4 times of the runner rotational frequency, a minimum of 6 revolutions of the runner has been chosen to observe at least one revolution of the vortex rope due to the computational limitations. Therefore the transient simulation was run for at least 6 complete rotation (≈1 s) of the runner and the selected time step size was 0.5° runner rotation, t=1.27E-6 s.

High-resolution advection scheme was applied for the continuity and momentum equations. A second order backward Euler scheme was used for time. Standard k-ε turbulence model and SST k-ω model were used to simulate the turbulence in the flow domain. The convergence criteria were set as RMS for pressure, mass-momentum, and turbulent parameters below 10E-5 [22, 24-25]. The solution was converged in each iteration through each inner loop. The number of inner loops was set to 10 for achieving the desired accuracy.

Results and Discussions

Numerical results were obtained and compared with the experimental data of Trivedi C. et al. 2013 [3] for the average and variation of the pressure, flow parameters, and frequency spectrum. Iso-surface of the pressure in the draft tube was generated to visualize the vortex rope formation.

Hydraulic efficiency and average pressure

Table 3 shows the experimental and numerical (k-ε and SST) hydraulic efficiencies for different operating conditions. The minimum differences between experimental and numerical hydraulic efficiencies are observed from the standard k-ε turbulence model at all operating conditions. The present paper is focused on the upper part load condition ($\alpha = 6.72°$, $Q =0.126$ m^3 s^{-1}) of turbine where the difference between the experimental and numerical efficiencies is 4.3% and 5.2% for k-ε and SST, respectively.

Table 3 Experimental and numerical hydraulic efficiency at different operating conditions

Operating condition		Hydraulic efficiency, η_h (%)		
GVO ($\alpha°$)	Q (m^3 s^{-1})	Experimental	Numerical	
			Standard k-ε	SST k-ω
3.91	0.070	72.3	80.5	82.4
6.72	0.126	89.0	93.3	94.2
9.84	0.200	93.4	94.1	94.9
12.44	0.220	91.2	93.8	94.5

Average pressure at the selected specific points of the turbine (see Fig. 2) were used to determine the difference between the numerical and experimental pressure values. The numerical pressure data were averaged using samples collected over six complete revolutions of the runner after achieving periodic flow condition. The variation of average experimental and numerical pressure values from the vaneless space to the draft tube are shown in Fig. 5. The numerical pressure values obtained with both standard k-ε model and SST k-ω show small difference with the experimental values. The numerical pressure values are higher (~2.8%) than the experimental values at the vaneless space and runner locations. In the draft tube locations, the numerical pressure values are about 5% lower than the corresponding experimental values. The maximum pressure values are observed at the vaneless space for both experimental (170 kPa) and numerical (175 kPa) data. Circumferential static pressure distribution in the vaneless space before the runner inlet is shown in Fig. 6. The average pressure in the stay vanes row is 219 kPa and decreased to ~175 kPa in the vaneless space with the flow acceleration between the guide vanes.
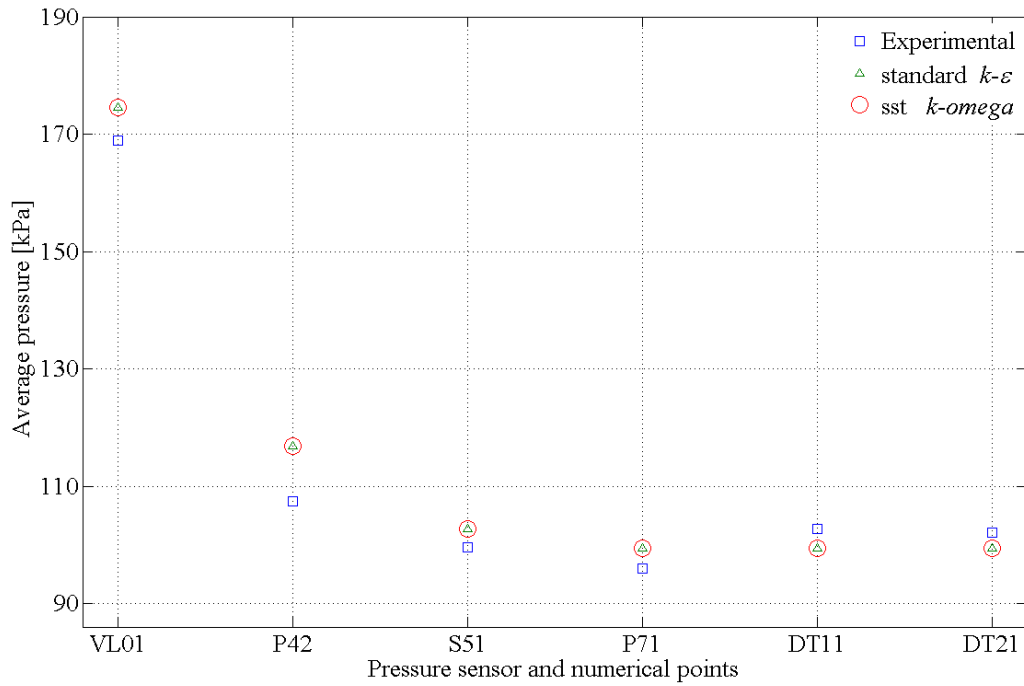
Fig. 5 Comparison of experimental and numerical average pressure values at different locations in the turbine (Q=0.1265 $m^3 s^{-1}$).VL01-Vanelees space, P42-Blade pressure side, S51-Blade suction side, P71- Blade trailing edge, DT-Draft tube.

Figure 7 shows the static pressure distribution from the leading edge to the trailing edge at the pressure side of a blade. The average pressure is 167.50, 118.02 and 98.02 kPa at the leading, half-length and trailing edge of the blade, respectively. This indicates that most of the pressure energy is transferred in the first half of the 15 blades and 15 splitters. At the draft tube locations, DT11 and DT21, the experimental and numerical pressure values are 103 kPa and 100 kPa, respectively. The numerical pressure values in the draft tube are 1% lower than that of the experimental measurements. This is the minimum pressure difference observed between the experimental and numerical results among of all the observed points in the turbine. As both of turbulence models (Standard k-ε and SST k-ω) presents almost similar pressure results, the results in the next section is presented using standard k-ε model as suggested by Trivedi et al.2013 [3].
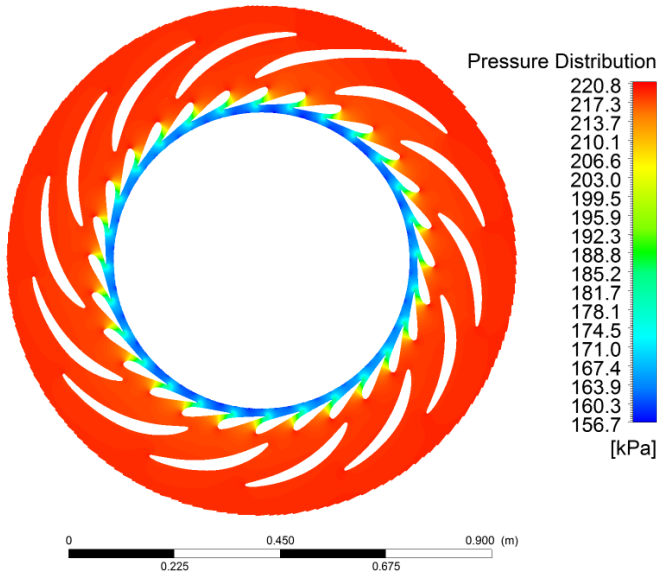
Fig.6 Circumferential static pressure distribution in the stay vanes, guide vanes
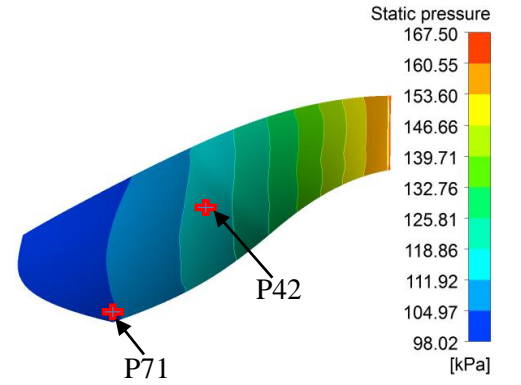
Fig.7 Static pressure loading on the runner blade surface

Pressure fluctuations

The pressure fluctuations inside the turbine with respect to the runner angular position have been investigated. The acquired pressure signals ($\tilde{p}$) was subtracted from its mean pressure ($\overline{p}$) to obtain the fluctuating pressure (p^*) using equation 1.

$$p^* = \tilde{p} - \overline{p} \qquad \text{[kPa]} \qquad (1)$$

A band-stop filter was designed to filter out the frequencies related to the system excitations and noise as shown in equation 2.

$$H_{BS}(f) = \begin{cases} 1, F_{c1} \leq f \leq F_{c2} \\ 0, \text{otherwise} \end{cases} \qquad (2)$$

Where $H_{BS}(f) = H_{LP2}(f) - H_{LP1}(f)$, $H_{LP2}(f)$ and $H_{LP1}(f)$ are low-pass filters with the lower and upper cut-off frequency F_{c1} and F_{c2}, respectively and, f is the frequency in pressure-time raw signal.
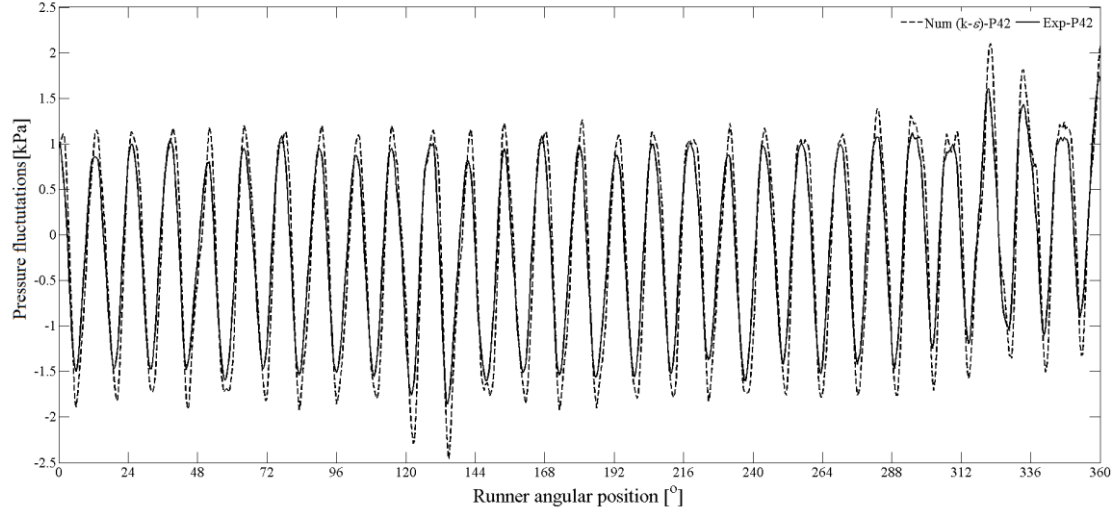
The extracted experimental and numerical pressure fluctuations at the locations VL01, P42 and DT11 are shown in Fig. 8 (a-c) at RSI frequency. At VL01, pressure fluctuations with 30 peaks during one complete rotation of the runner correspond to the blade passing frequency (see Fig. 8(a)). The

amplitude of the instantaneous pressure fluctuations for the numerical data was approximately 13% higher than the corresponding experimental values. The 28 peaks observed at the location P42 correspond to the guide vane passing frequency (see Fig. 8(b)). The amplitude of the instantaneous pressure peaks observed for the numerical signal was approximately 14% higher than for the corresponding experimental values. The maximum amplitude was observed as ±1.142 kPa for the experimental pressure signal. The draft tube pressure signal from DT11 had also 30 pressure peaks in both numerical and experimental pressure signals. This indicates that the pressure fluctuations developed by the runner blades (30) wakes propagate downstream the runner (see Fig. 8(c)). The maximum amplitude for the numerical pressure fluctuations was 0.09 kPa, which was approximately 12% higher than the corresponding experiment values.

Several pressure peaks near to the blade passing frequencies were observed at this operating condition, which confirm the unsteadiness in the flow. Therefore, further investigations were carried out by fast Fourier analysis (FFT) which is presented in the next section. The irregularities in the shape of the pressure peaks were observed due to the unsteady flow leaving the guide vane trailing edge and entering the runner which was giving sudden drop to the pressure on the blade surface after the runner inlet [3].
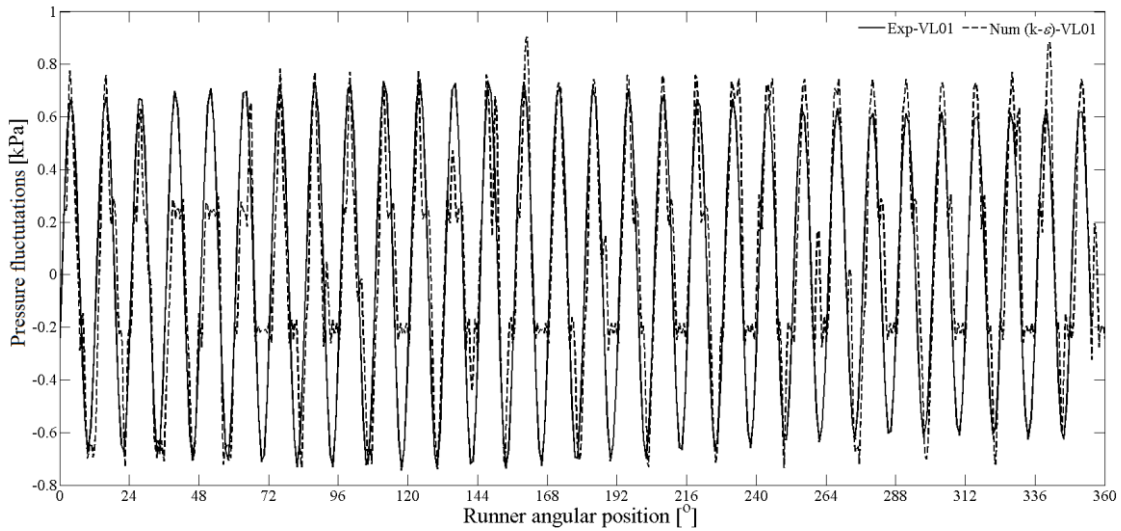

(a)

(b)
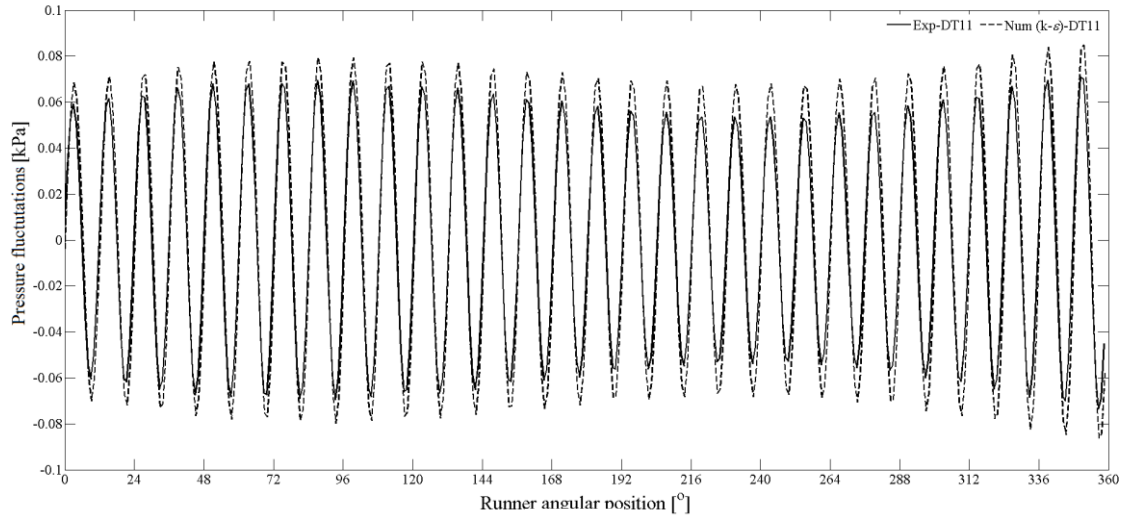
(c)

Fig. 8 Experimental and numerical time-averaged pressure signals at part load operating condition for the rotor stator interaction. (a)VL01, (b) P42, (c) DT11. VL01-Vanelees space, P42-Blade pressure side, DT-Draft tube.
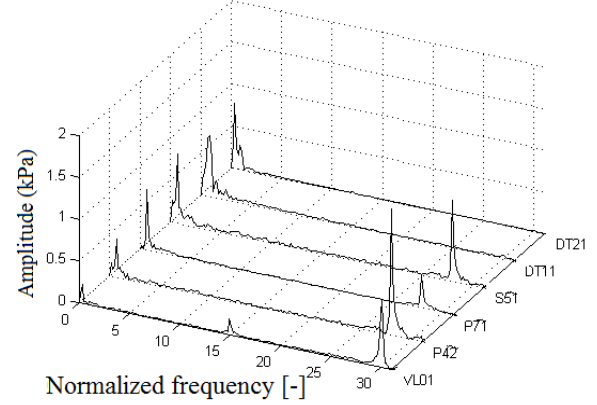
Spectral analysis

The spectral analysis of both the experimental and numerical pressure-time signals was carried out using a Matlab-Spectrum Pwelch algorithm and is presented in Fig. 9. The x-axis represents the normalized frequencies and y-axis represents the amplitude of the pressure signal. The frequencies were normalized using Eq. 3.

$$f^* = \frac{f}{f_n}[-]$$

(3)
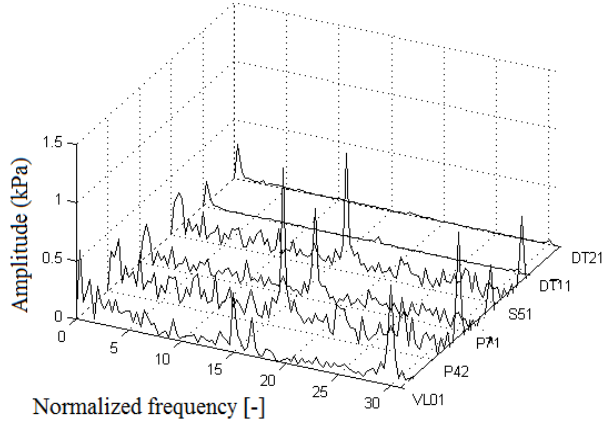
(a) Experimental   (b) Numerical

Fig. 9 Fast Fourier transformation of numerical pressure signals. VL01-Vanelees space, P42-Blade pressure side. VL01-Vanelees space, P42-Blade pressure side, S51-Blade suction side, P71- Blade trailing edge, DT-Draft tube.

Non-dominant normalized frequencies of the numerical pressure signals were filtered out by designing a multiband cascade of band pass filters in MATLAB and plotted as shown in Fig 10. The rest of the normalized frequencies related to turbulence model discrepancies were ignored from the pressure signals. The amplitude of 0.85 kPa was observed in the vaneless space at the normalized frequency of 30, which corresponds to the blade passing frequency. The obtained amplitude of the blade passing frequency is approximately 13% higher than the experimental value. A normalized frequency of 0.30 can be seen at the location VL01, which corresponds to the helical vortex frequency in the draft tube. The observed amplitude is very low but shows good agreement with the experimental value, with difference within 3.9%. At the locations P42, P71 and S51, the normalized frequency of 28 is observed which corresponds to the guide vane passing frequency and harmonics. The normalized frequency of 0.7 is observed in the runner which corresponds to the vortex breakdown. The vortex breakdown frequency in the runner is obtained by subtracting the vortex breakdown frequency from the runner rotational frequency as they are co-rotating.
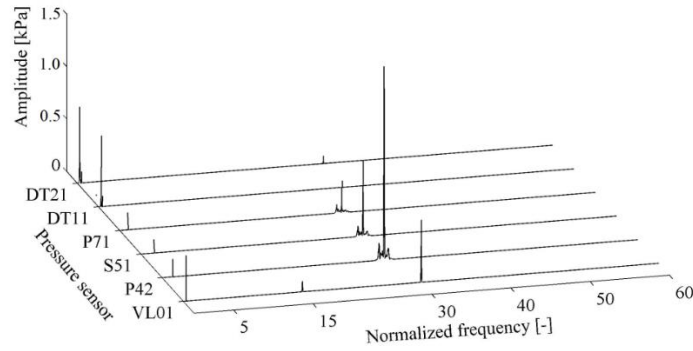
Fig.10 Filtered frequency spectrum of the numerical pressure-time domain signals at 50 % load.
VL01-Vanelees space, P42-Blade pressure side, S51-Blade suction side, P71- Blade trailing edge,
DT-Draft tube.

Vortex rope identification

The SST k-ω model better predicts turbulence in the flow in case of boundary layers are fully developed. . Fully developed boundary layers are difficult to obtain in case of Francis turbine due to high pressure gradients and complex shape of geometry. Therefore, both turbulence models, Standard k-ε and SST k-ω, were used in the present study to observe the turbulence in draft tube and to identify the model which is capable to predict the vortex break down in the draft tube at PL operating condition. The turbulence kinetic energy (TKE) plot for both the turbulence models are shown in Fig. 11. Both the turbulence models are capable of predicting the vortex rope in the draft tube.
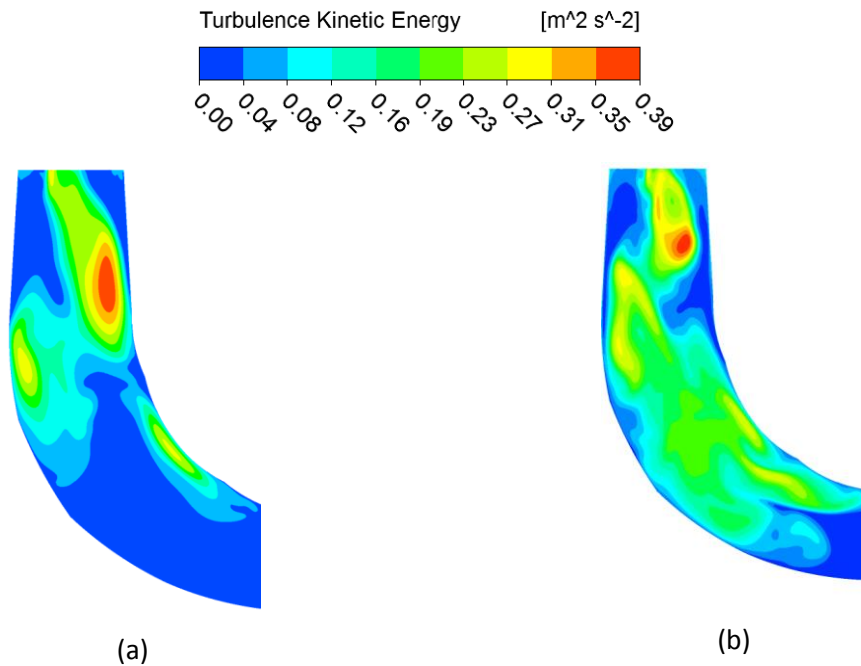

(a)   (b)

Fig. 11 Turbulent kinetic energy of swirling flow in the elbow draft tube with two turbulence models at PL operating condition; (a) Standard k-ε, (b) SST k-ω

Results from both the models were analyzed and the significant variation in turbulence kinetic energy is observed due to swirl induce by turbine part load operating condition. Generally, for a Francis turbine, there is no swirl at the inlet of the turbine but at the outlet; the swirl will vary as the load changes. The variation in the turbulence kinetic energy with k-ε and SST turbulence models at part load operating condition can be clearly seen from the Fig.11. The SST turbulence model is capable to resolve the multiple length scale eddies since it does not employ the damping function as k-ε turbulence model. This can be observed in Fig. 11 (b) as multiple eddies are resolved by the SST turbulence model in the draft tube cone and elbow, whereas, k-ε turbulence model almost dampened the eddies of draft tube elbow. The clear shape of the vortex rope is observed with standard k-ε model because it resolves the single length scale eddies. The frequency of the vortex rope is observed same fromboth turbulence models.The shape of the clear vortex rope obtained from Standard k-ε model is shown in Fig.13. Therefore, in continuation to previous analysis, the detailed analysis in the next paragraph is presented using standard k-ε to compare the experimental results.

Numerically obtained pressure values at the locations DT11 and DT21 showed the normalized frequency of 0.3 which corresponds to the vortex rope. In additon to the vortex rope frequency the main challenge of the numerical analysis is the prediction of the pressure pulsation amplitudes for the part load operating conditions. The comparison between the experimental and the numerical results shows that the numerical prediction of the position of the maximum pressure pulsation amplitude is reasonably accurate, but the predicted values of the amplitudes are lower than that of the experimental ones as shown in Fig.12.
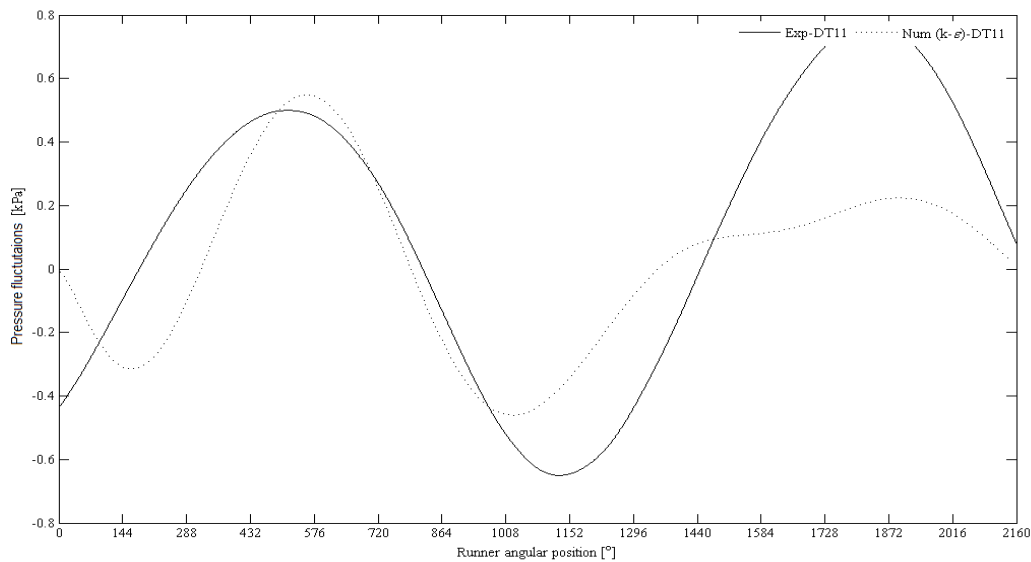

Fig. 12 Numerical and experimental pressure signals with respect to the runner angular position in draft tube at DT11
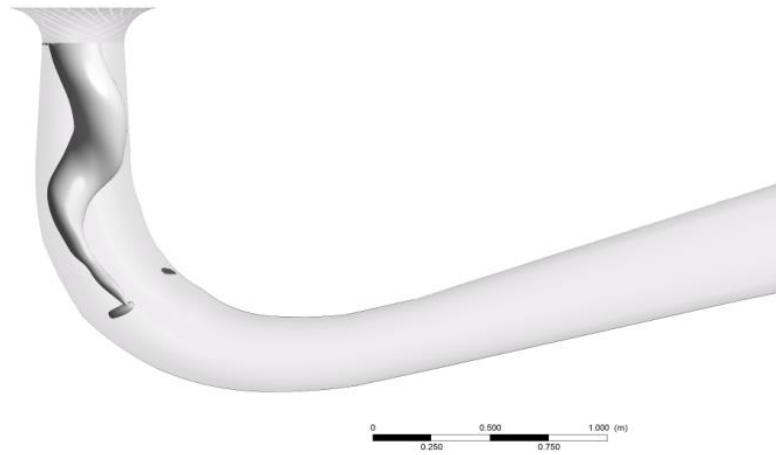
Fig.13 Iso-surface of constant pressure in draft tube at a pressure of 98.5 kPa

The shape of the vortex rope is presented as iso-surface of constant pressure of 98.5 kPa in Fig.13. The rope is co-rotating with the runner. The vortex rope has the shape of a rotating cork-screw. The velocity streamlined across the cross-section of the draft tube are shown in Fig.14. The shape of the streamlines indicates the rotating vortex rope inside the draft tube. At the inlet of the draft tube, the flow entered with high velocity, decreasing continuously towards the outlet of the draft tube. A draft tube is designed to recover the kinematic energy leaving the runner into pressure; as the pressure recovers along the draft tube, the velocity reduces.
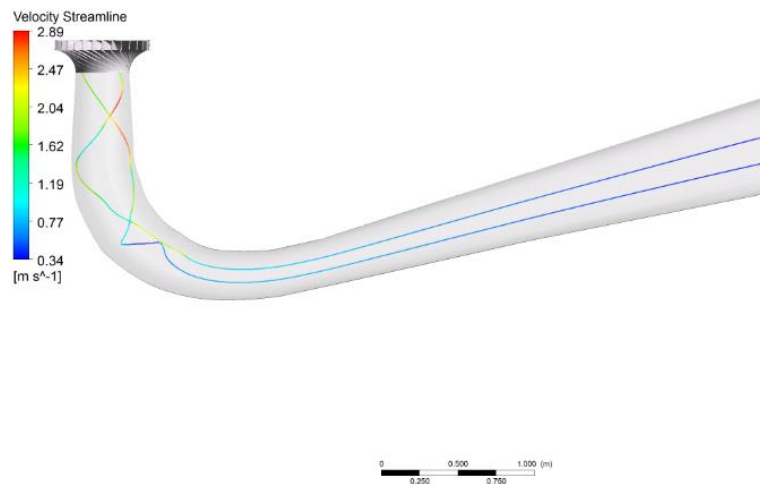

Fig.14 Velocity streamlines across the cross section of the draft tube

Pressure distribution along the draft tube mid-plane is shown in Fig.15. The low pressure region generated at the draft tube center originates from the swirling flow leaving the runner. The vortex rope in the draft tube is generally wrapped around this low pressure region.. The observed

average pressure at the inlet of the draft tube was 95 kPa and 100 kPa at the outlet of the draft tube. The pressure recovery is low as expected; at the PL operating point, effect of vortex breakdown and flow seperation is strong. This results in adverse pressure gradient in the boundary layer of draft tube wall and reattachment of the seperated flow does not occur. Moreover, pressure gradient from center of the draft tube to the wall is large and it changes constantly with the runner angular movement. Low pressure zone at the center of the runner outlet can be seen that correspond to the vortex core.
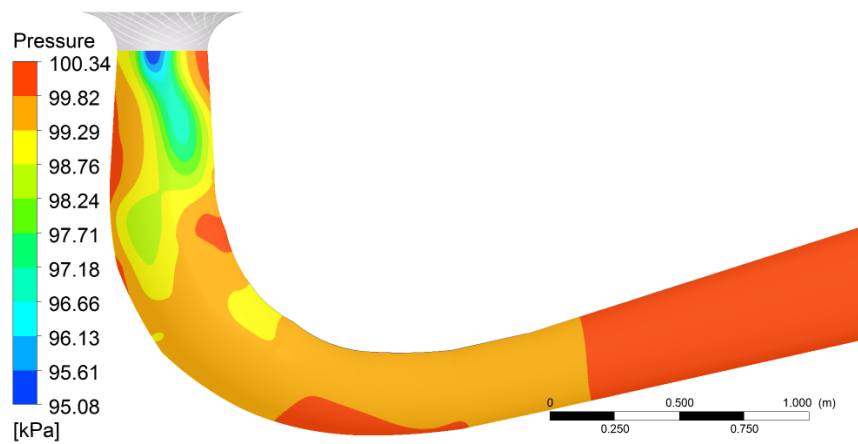

Fig.15 Average pressure variation in the draft tube at PL operating condition; the pressure contours correspond to an instantaneous runner position at the end of unsteady simulation.

Figure 16 shows the vectors on the mid-plane of the draft tube. Two vortices can be observed in the draft tube. One of the vortices (marked I) is closed to the draft inlet and the second (marked II) is near the exit of the draft tube cone which blocks the flow in the draft tube. The eddies were also observed as regions of high turbulence kinetic energy (see Fig. 11a). The eddies cause large disturbance in the vector field directions and induces losses in the draft tube (cone) by increasing the velocity of the flow around.
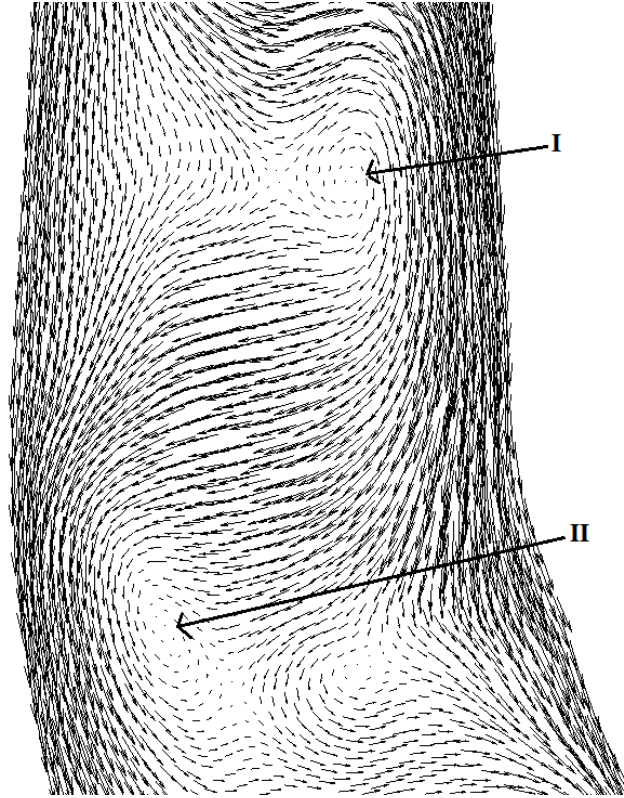
Fig.16 Vector field in the draft tube at PL operating condition; I and II are vortices in the draft tube cone

Conclusions

In order to investigate the flow phenomena in the vaneless space, runner, and draft tube at 50% load of a high head model Francis turbine, unsteady numerical simulation has been performed. The complete model is simulated from the spiral inlet to the draft tube outlet by solving unsteady RANS equations with Standard k-ε and SST k-ω turbulence models. The comparison of numerical and experimental average pressure values inside runner, vaneless space and draft tube shows reasonably good agreement for both the turbulence models and Standard k-ε turbulence model was used for further investigations since it gives better prediction of numerical prediction of hydraulic efficiency.

Unsteady pressure fluctuations obtained in the vaneless space were high with the maximum amplitudes occurring at the blade passing frequency. Interestingly, small variation in the pressure amplitude related to the splitter blade was observed in comparison to that by the main blades.

In the draft tube, high amplitudes were observed at two different frequencies, blade passing frequency and the vortex breakdown frequency, the later being higher. The draft tube instabilities were affected by the large and small vortical flow structures at the outlet of the runner because the pressure pulsations in the draft tube were developed by the fluid flow dynamics. It is seen that the vortex rope is developed due to the vortex beak down at draft tube inlet The effect of vortex break down frequency was observed decreasing upstream and diminishes after a short distance upstream of spiral casing inlet. To resolve the dynamics of flow completely we are further looking for upcoming experimental measurements with particle image velocimetry (PIV) and subsequent numerical simulation.

References

1. Trivedi, C., Gandhi, B., Cerventes, M. J., Effect of transients on Francis turbine runner life: a review. Journal of hydraulic research Vol. **51**, Issue 2. dOI:10.1080/00221686.2012.732971 (2013)

2. Liu, Y. Z., Chen, H. P., Koyama, H.S., Joint investigation of rotating flow with vortex breakdown using CFD, visualization and LDV. Journal of Hydrodynamics, **17(4)**, pp. 455-458 (2005)

3. Trivedi, C., Cerventes, M. J., Gandhi, B., and Dahlhaug O. G., Experimental and Numerical Studies for a High Head Francis Turbine at Several Operating Points. Journal of Fluids Eng. 2013, **135(11)**, pp. 111102. doi: 10.1115/1.4024805 (2013)

4. Wang F.-j., Li X.-q., and Ma, J.-m., and Yang, M., Experimental investigation of characteristic frequency in unsteady hydraulic behaviour of a large hydraulic turbine .Journal of Hydrodynamics, Vol. **21(1)**, pp. 12- 19 (2009)

5. Keck, H. and Sick, M., Thirty Years of Numerical Flow Simulation in Hydraulic Turbomachines", Acta Mech, Vol. **201**, pp. 211-229, Doi:10.1007/s00707-008-0060-4 (2008)

6. Liu, X.-b. and Zeng Y.-z., Numerical prediction of vortex flow in hydraulic turbine draft tube for LES, Journal of Hydrodynamics, Ser. B, Vol.17 (4), pp. 448-454 (2005)

7. Brekke, H., A Review on Oscillatory Problems in Francis Turbine. New Trends in Technologies: Devices, Computer, Communication and Industrial Systems, ISBN-978-953-307-212-8, Chapter-**12**, pp.217-232 (2010)

8. Nicolet, C., Hydroacoustic Modelling and Numerical Simulation of Unsteady Operation of Hydroelectric Systems, PhD thesis No **3751**. École Polytechnique Fédérale de Lausanne (2007)

9. Staubli, T., Senn, F., and Sallaberger, M., Instability of Pump-Turbines during Start-up in the Turbine Mode. Hydro , Ljubljana, Slovenia (2008)

10. Xiao, Y. X., Wang Z., Yan, Z., Experimental and Numerical Analysis of Blade Channel Vortices in a Francis Turbine Runner. International Journal for Computer-Aided Engineering and Software. Vol. **28 (2)**, pp.154-171 (2011)

11. Hasmatuchi, V., Farhat, M., Roth, S., Botero, F., and Avellan, F., Experimental Evidence of Rotating Stall in a Pump-Turbine at Off-Design Conditions in Generating Mode. ASME Journal of Fluids engineering, Vol. **133(5)**, 051104, pp. 1-8, doi:10.1115/1.4004088 (2011)

12. Zobeiri, A., Kueny, J.-L., Farhat, M., and Avellan, F., Pump-Turbine Rotor-Stator Interactions in Generating Mode: Pressure Fluctuation in Distributor Channel. *23rd IAHR Symposium*, October 2006, Yokohama, Japan, pp. 1-10 (2006)

13. Zhang, R.-K. et al., Characteristics and Control of the Draft-Tube Flow in Part-Load Francis Turbine. ASME Journal of Fluids Engineering, Vol. **131(2)**, 021101, pp. 1-9, doi:10.1115/1.3002318 (2009)

14. Ruprecht, A., Simulation of Vortex Rope in Turbine Draft Tube. Proceedings of Hydraulics Machinery Systems. *21st IAHR symposium*, Lausanne (2002)

15. Minakov, A. V., Platonov, D.V, Dekterev, A.A., Sentyabov, A.V., and Zakharov. A.V., The Numerical simulation of low frequency pressure pulsations in the high-head Francis turbine. Computers & Fluids, Vol. **111**, pp. 197-205, doi:10.1016/j.compfluid.2015.01.007 (2015)

16. Nicolet, C. et al., Methodology for Risk Assessment of Part Load Resonance in Francis Turbine Power Plant. IAHR International Meeting of WG on Cavitation and Dynamic Problems in Hydraulic Machinery and Systems, Barcelona, Spain, pp. 1-16 (2006)

17. Cerventes, M. J., Andersson, U., and Lövgren, H. M., Turbine-99 Unsteady Simulations – Validation. IOP Conference Series: Earth and Environmental Science, Vol. **12(1)**, 012014, pp. 1-10, doi:10.1088/1755-1315/12/1/012014 (2010)

18. Susan-Resiga, R., Ciocan, G. D., Anton, I., and Avellan, F., Analysis of the Swirling Flow Downstream a Francis Turbine runner. ASME Journal of Fluids engineering, Vol. **128 (1)**, pp. 177-189, doi:10.1115/1.2137341 (2005)

19. Buntic, O. I., Dietze, S., and Ruprecht, A., Numerical Simulation of the Flow in Turbine-99 Draft Tube. Turbine-99 III, *Proceedings of the third IAHR/EROCOFTAC workshop on draft turbine flow*, Porjus, Sweden (2005)

20. Wallimann, H., and Neubauer, R., Numerical study of a high head Francis turbine with measurements from the Francis-99 project. Journal of Physics: Conference Series, **579(1)**, p. 012003. doi: 10.1088/1742-6596/579/1/012003 (2015)

21. Wu, J., Shimmei, K., Tani, K., Niikura, K., and Sato, J., CFD-Based Design Optimization for Hydro Turbines. ASME Journal of Fluid Engineering, Vol. **129(2)**, pp. 159-168, doi:10.1115/1.2409363 (2007)

22. Ciocan, G. D., Iliescu, M. S., Vu, T. C., Nennemann, B., and Avellan, F., Experimental Study and Numerical Simulation of the FLINDT Draft Tube Rotating Vortex. ASME Journal of Fluids Engineering, Vol. **129(2)**, pp. 146-158, doi:10.1115/1.2409332 (2007)

23. Staubli, T. and Meyer, D., Draft Tube Calculations. Turbine 99, *EROCOFTAC/IAHR Workshop on Draft Tube Flow*. Porjus, Sweden (1999)

24. Luis, C., Eduardo, O. d. S., Marcelo, D. d. M., and Antonio, C. P. B. J., Assessment of Turbulence Modelling for CFD Simulations into Hydroturbines: Spiral Casing. *17th International Mechanicsl Engineering Congress (COBEM)*, Sao Paulo, Brazil (2003)

25. Widmer, C., Staubli, T., and Ledergerber, N., Unstable Characteristics and Rotating Stall in Turbine Brake Operation of Pump-Turbines. ASME Journal of Fluids Engineering, Vol. **133(4)**, 041101, doi:10.1115/1.4003874 (2011)

26. Mossinger, P., Jester-Zurker, R., and Jung, A., Investigation of different simulation approaches on a high-head Francis turbine and comparison with model test data: Francis-99. Journal of Physics: Conference Series, **579(1)**, p. 012005. doi: 10.1088/1742-6596/579/1/012005 (2015)

27. Jost, D., Skerlavaj, A., Morgut, M., Meznar, P., and Nobile, E., Numerical simulation of flow in a high head Francis turbine with prediction of efficiency, rotor stator interaction and vortex structures in the draft tube. Journal of Physics: Conference Series, **579(1)**, p. 012006. doi: 10.1088/1742-6596/579/1/012006 (2015)

28. Goyal R., Trivedi, C., Gandhi, B., Cerventes, M. J., and Dahlhaug O. G., Transient pressure measurements at part load operating condition of a high head model Francis turbine. Sadhana, Springer (Revised manuscript submitted) (2015)